Sensors and Materials, Vol. 36, No. 3 (2024) 1065–1079
MYU Tokyo

S & M 3581

Application of Motor Current Measurement Technology in Propeller Cutting by Robotic Arms

Yuan-Ming Cheng,[1*] Gu-Ming Chang,[2] and Yu-Hao Chang[2]

[1]Department of Intelligent Robotics, National Pingtung University, Pingtung 90004, Taiwan, Republic of China
[2]Department of Computer Science and Information Engineering, National Pingtung University, Pingtung 90004, Taiwan, Republic of China

(Received November 21, 2023; accepted March 6, 2024)

Keywords: motor current, cutting force, force sensors, robotic arm, propellers

Propellers comprise fan-shaped structures with spiral blades. The real-time measurement of cutting and grinding forces during the milling and grinding of propellers is difficult to achieve. The spindle motor current is a common parameter used to measure cutting force. However, data related to this parameter are not accessible during the use of DC motors for cutting processes and can be obtained only from servo motor drive systems. Given these considerations, in this study, we adopted LabVIEW software to develop a program for use in combination with an inexpensive sensor to achieve the simultaneous measurement of the cutting force and motor current. The program was verified to accurately depict the relationship between the cutting force and the motor current of reconfigurable precision five-axis machine tools, rendering it a viable alternative to measurement schemes that rely on expensive force sensors. Subsequently, the developed program was further tested by measuring changes in spindle motor current while cutting three blades to produce a 3D-printed polylactic acid propeller.

1. Introduction

A propeller is a rotating device used to propel fluid, with blades being the primary working components of the propeller. They are typically flat and have a relatively large surface area, fixed onto a central shaft and arranged at specific angles and orientations according to particular design specifications. The shape and quantity of the blades can be adjusted on the basis of the purpose and design of the propeller.

Propeller casting involves 13 processes starting from wax injection to detail polishing. Figure 1 presents a flowchart of propeller precision casting. Of the processes involved, grinding has the most labor-intensive tasks because propellers are composed of multiple 3D blades with curved surfaces and thus can be created only by experienced craftsmen, who must polish and grind each workpiece according to its required characteristics. Nagata *et al.*(1) implemented a force control scheme to maintain the contact force between a workforce and a polishing tool held by robotic arms. Dong *et al.*(2) developed a control scheme with a six-axis robotic arm to

*Corresponding author: e-mail: Chengym@mail.nptu.edu.tw
https://doi.org/10.18494/SAM4787

ISSN 0914-4935

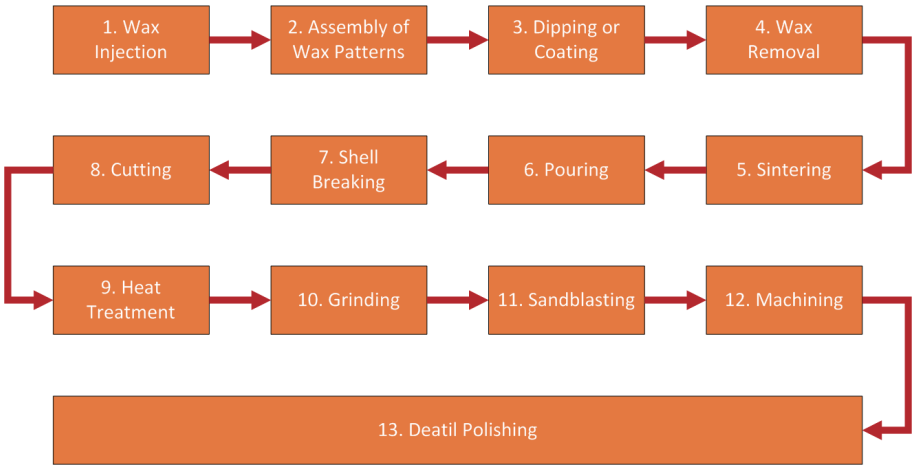

Fig. 1. (Color online) Flowchart of propeller precision casting.

complement an automatic hardware polishing system. This scheme maintains the workpiece-tool contact force within a specific range by extracting motor current data related to the polishing wheel; these data then undergo analog-to-digital conversion and are input into a proportional-integral-derivative controller to achieve real-time compensation.

The fully automated and smart production of propellers requires the accurate measurement and control of cutting and grinding forces during polishing. At present, most available control schemes involve the installation of six-axis force sensors on the end effectors of robotic arms. However, such sensors are not only expensive but also limited by task assignment and load constraints. In addition, the installation of force sensors on a robotic arm affects the arm's operation and load capacity. In previous studies,[3–5] the cutting force was measured by measuring the feed drive motor current. To considerably reduce costs, in this study, we adopted an inexpensive current sensor to measure the spindle motor current and estimate the cutting force.

Altintas[3] monitored milling processes by measuring the feed drive motor current and established a feed drive control system model to analyze the measurement values of the cutting force exerted by the drive motor and thus predict cutting force and tool breakage. Aslan and Altintas[4] used the Denavit–Hartenberg method to establish a kinematic model for a five-axis machine tool to predict the cutting force of this tool on the basis of its feed drive current. The feed drive motor current of a machine tool provides a substantial amount of information regarding machining states. During milling, the bandwidth of a current sensor is related to the spindle speed or cutting tool rotation speed. Jeong and Cho[5] used an empirical approach to expand the current sensor bandwidth to 130 Hz.

Cutting force has a considerable effect on workpiece quality and cutting tool lifespan. Thus, the online monitoring of cutting tool wear conditions is a crucial research area in the field of automatic machining. Such monitoring ensures adequate workpiece size and precision, and prevents damage to cutting tools. Tanabi *et al.*[6] measured the feed drive motor current and used it as the input for a fuzzy logic scheme to develop an online monitoring system for determining

damage to cutting tools. Miura *et al.*[7] developed a cutting force control scheme by installing external voltage and current sensors on the feed drive motor of a machining center to monitor cutting force. This scheme was evaluated through a cutting test and compared with a dynamometer-based method. Li *et al.*[8] used an inexpensive current sensor installed on the AC servomotor of a computerized numerical control tuning center to monitor the wear conditions of cutting tools. In that study, the authors used neuro-fuzzy techniques to model a feed drive system and create a framework for estimating the feed cutting force according to the measured feed drive motor current. Matsubara and Ibaraki[9] explored multiple methods for collecting cutting force data, including real-time measurement, offline measurement, online measurement, and online monitoring approaches. They also introduced common data processing and analysis techniques including filtering, feature extraction, and mode recognition. Finally, they determined several useful approaches and strategies for cutting force monitoring and control including relevant algorithms, self-adaptive control schemes, and optimized control methods.

In this study, an inexpensive current sensor was installed on a DC spindle motor and a force sensor was installed on a reconfigurable precision five-axis machine tool (RPFMT).[10,11] A program developed in LabVIEW was used to simultaneously record current data obtained by the current sensor and cutting force data obtained by the force sensor; this approach constitutes an inexpensive alternative to force measurement methods that involve costly equipment. Four cutting experiments, each with unique cutting conditions (i.e., feed rate, cutting depth, up milling, and down milling), were performed to determine the relationship between the cutting force and the spindle motor current. Subsequently, another experiment was performed using RoboDK software to plan the cutting path of a six-axis robotic arm and physically create a propeller. Because the propeller in question comprised three blades attached to a single rotating spindle, the cutting path needed to be formulated for only a single blade; the machining of the remaining two blades was achieved by rotating the spindle. Accordingly, the DC motor current of the robotic arm was measured in this experiment to derive the corresponding cutting force.

2. Experimental Setup

The RPFMT examined in this study comprises a 3-prismatic-revolute-spherical (3-PRS) parallel motion platform and an XY motion platform (Fig. 2). The 3-PRS platform has three degrees of freedom (Z, α, and β) and features a simple mechanism with high rigidity, high precision, and low inertia. The spindle motor examined in this study was an HSM-90 spindle motor (ToolmakerIND) with a voltage of 110 V, a rotation speed of 25000 RPM, and an input force of 230 W. In the experiments, the diameter of the cutting tool was 6 mm.

In this study, we employed a PCB208C01 force sensor, a high-precision quartz sensor with stainless-steel casing, and a voltage-resistant quartz-sensing element. This element has extremely high hardness, enabling the sensor to be positioned between the bottom plates of machining tools.

The NI9234 signal acquisition module and cDAQ-9171 chassis used in this study were developed by National Instruments. The module can acquire signals that do not adhere to the integrated electronics piezoelectric standard, such as those recorded by accelerometers and

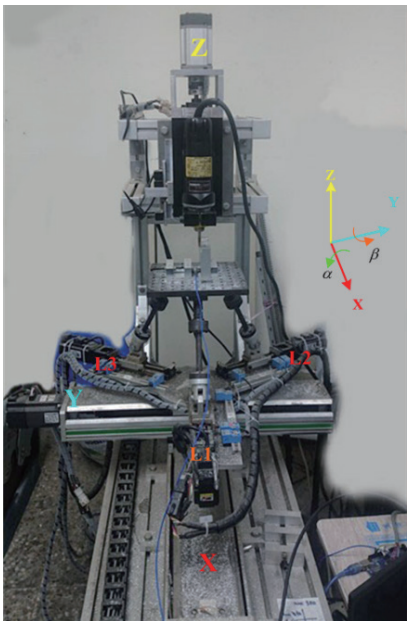

Fig. 2. (Color online) RPFMT.

tachometers. In addition, the module provides a wide dynamic range and features built-in software for AC/DC matching and for the processing of integrated electronics piezoelectric signals. The input channels of the module can simultaneously digitize signals. Finally, we employed cDAQ-9171, a CompactDAQ USB chassis that becomes operational immediately upon being connected to a device for data sensing and electronic measurement.

The PZEM-004T AC communication module employed in this study is mainly used to measure AC voltage, current, active force, frequency, force factor, and active energy. It utilizes a transistor–transistor logic (TTL) interface to read data, and its physical layer uses a universal asynchronous receiver transmitter (UART)-to-TTL communication interface with a baud rate of 9600, 8 data bits, 1 stop bit, and no parity check. For application layer protocol communication, the Modbus-RTU protocol was used.

The robotic arm used in this study is the YASKAWA MH5LF module, as shown in Fig. 3(a). YASKAWA MH5L has an additional translation axis (Y) and a rotation axis (γ). MH5LF has the advantages of small size, light weight, and space saving. Its repeatability (i.e., positioning precision) reaches ±0.03 mm and its maximum load capacity is 5 kg. For these reasons, it is frequently used in various of automation fields. Figure 3(b) shows the working range of the robotic arm YASKAWA MH5LF.

In general, the system framework proposed in this study is divided into two parts. First, a five-axis machining tool can be used in combination with a force sensor and an AC communication module to simultaneously observe changes in cutting force and motor current during cutting (Fig. 4) in order to determine the relationship between these two parameters.

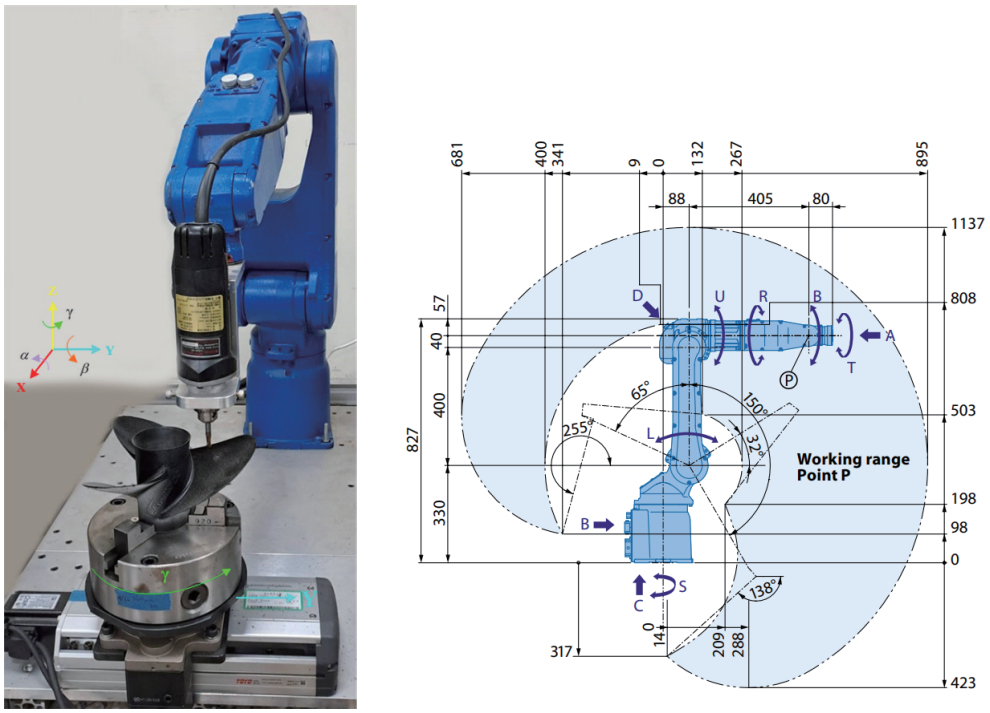

(a) (b)

Fig. 3. (Color online) (a) MH5LF robotic arm module. (b) Working range of the robotic arm YASKAWA MH5LF.

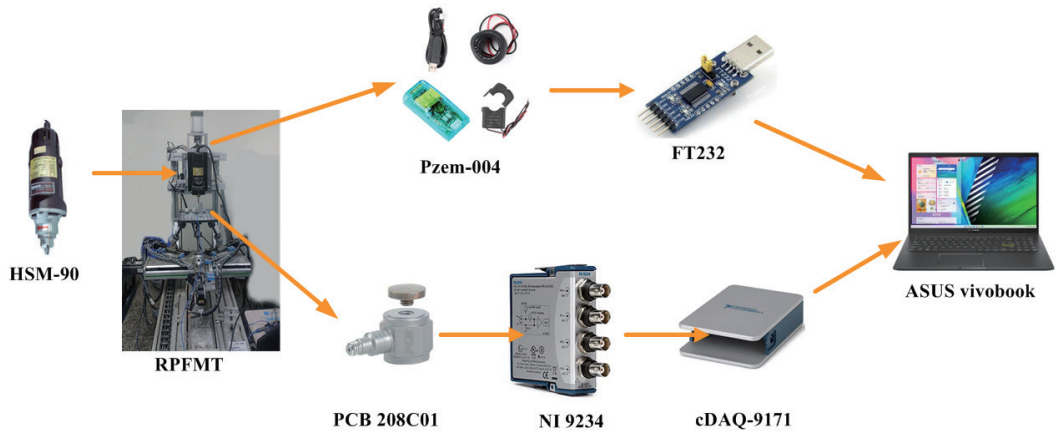

Fig. 4. (Color online) System framework for measuring cutting force and motor current.

Second, the developed program can be used to examine a robotic arm integrated with a communication module (Fig. 5). Changes in robotic arm current can be measured during polishing to determine whether the exerted cutting force is either excessively or insufficiently large. Table 1 presents the list of equipment used in the present cutting experiments.

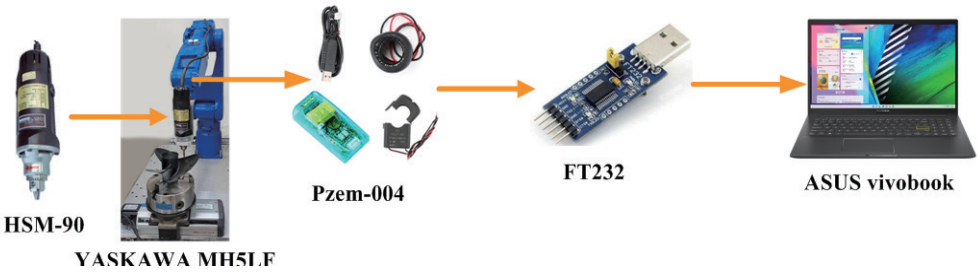

Fig. 5. (Color online) System framework for motor current measurement during cutting performed by a robotic arm.

Table 1
List of equipment for cutting experiments.

Name	Force sensor	CompactDAQ chassis	Signal acquisition module	UART-to-TTL interface	AC communication interface
Model no.	PCB 208C01	cDAQ-9171	NI 9234	FT232	PZEM-004T

3. Experimental Method

Figure 4 presents the system framework for the simultaneous measurement of the cutting force and motor current. In this study, the RPFMT was integrated with a force sensor and an AC communication module to measure changes in cutting force and motor current during cutting in order to determine the relationship between these two parameters. Figure 6 presents the program flowchart for such measurement.

Modbus-RTU was used as the protocol for monitoring the measurement of current data. The experiment confirmed that the query speed limit of PZEM-004T was 35 ms; the module then became unresponsive after the query speed was further increased. However, the response rate was highly unstable at 35 ms. Therefore, the query speed was set as 45 ms in the subsequent experimentation to ensure stability in data sampling.

The four cutting experiments (EXP1 to EXP4) were performed with the spindle motor HSM-90. Table 2 presents the experimental configuration of HSM-90. The fixed cutting parameters were a motor rotation speed of 25000 RPM, a cutting depth of 0.5 mm, a cutting width of 3 mm, and a sampling time of 45 ms. Figure 7 presents the cutting path of each experiment. The feed rates of EXP2 and EXP4 differed from those of EXP1 and EXP3 and varied on the basis of the numerical control (NC) code applied during cutting (Fig. 8). In the NC code, G56 was set as the initial position of the cutting process, during which the feed rate increased from F100 to F250 and then progressively decreased to F100 before the process was terminated. The relationship between changes in feed rate and current was examined during the experiments.

Figures 9(a) and 9(b) present the force and current data obtained from EXP1, respectively. The corresponding results revealed that when the force (i.e., cutting force) increased, the current increased instantaneously. Before cutting began (0–2.8 s), the spindle motor was idle, and its

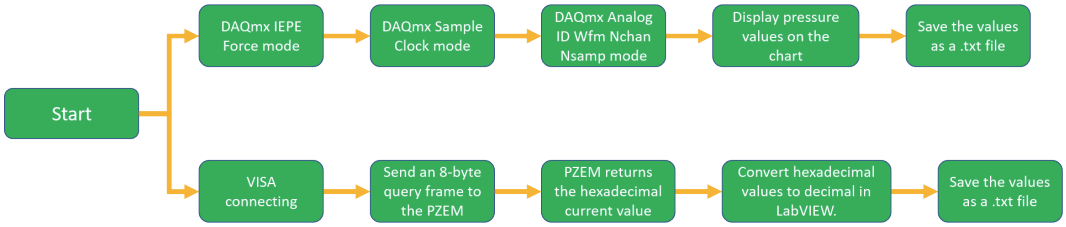

Fig. 6. (Color online) Flowchart for operation of the developed program.

Table 2
Experimental configuration of HSM-90.

Cutting tool type	Experiment no.	Feed rate (mm/s)	Cutting path
6-mm four-flute end mill	EXP1	100	Along the *y*-axis
	EXP2	Based on the NC code	Along the *x*-axis
6-mm two-flute ball end mill	EXP3	100	Along the *y*-axis
	EXP4	Based on the NC code	Along the *x*-axis

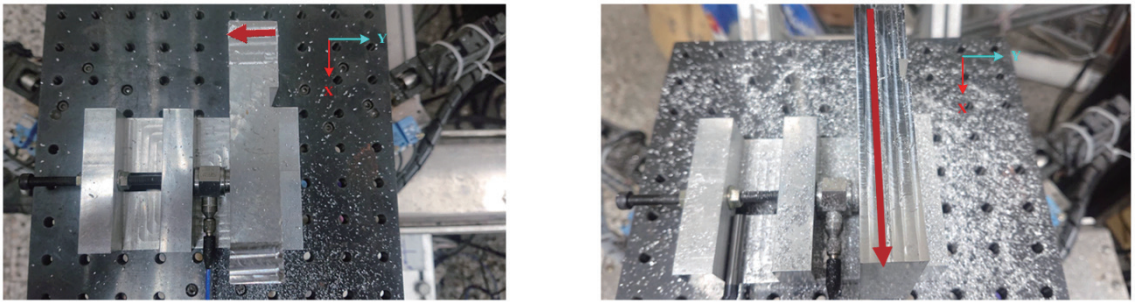

(a) (b)

Fig. 7. (Color online) Cutting directions. (a) Along the *y*-axis, with a feed rate of 100 mm/s. (b) Along the *x*-axis, with a feed rate based on the NC code.

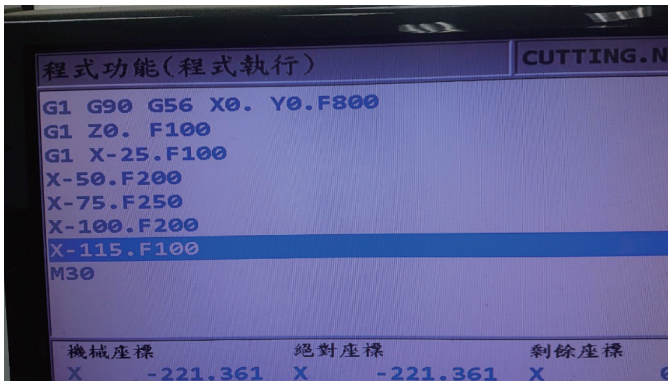

Fig. 8. (Color online) NC code with varying feed rates.

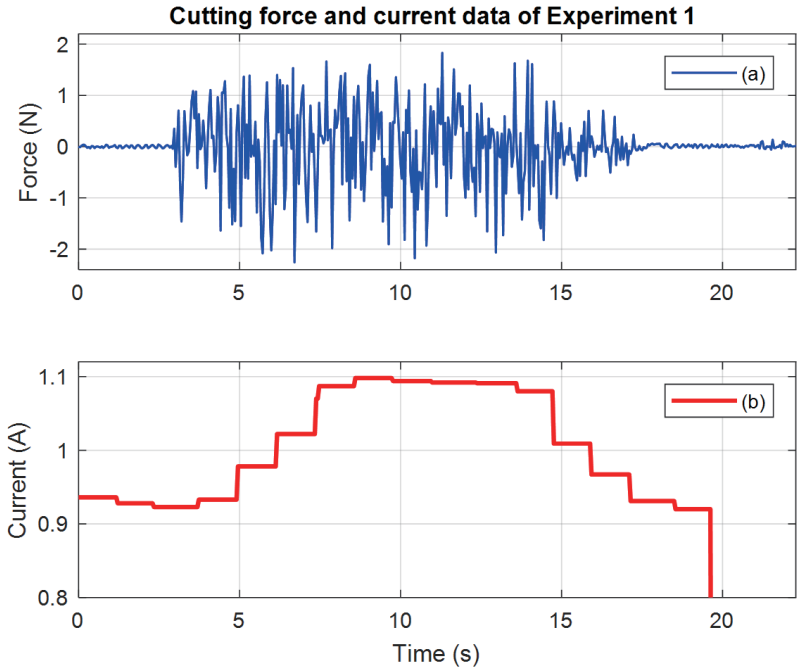

Fig. 9. (Color online) (a) Force and (b) current data of EXP1.

current was 0.94 A. After cutting began, the maximum cutting force and motor current reached 1.5 lbf and 1.1 A, respectively. Figures 10(a)–10(d) present the overall force, overall current, zoom-in force, and zoom-in current data obtained from EXP2, respectively. The cutting process of this experiment spanned 60 s. After the spindle motor was switched on, its rotation speed reached 25000 RPM, and the current progressively increased to 1.45 A and then decreased and stabilized at 1 A. During the stable cutting (13–50 s), the motor current remained stable at 1 A. When the feed rate decreased to 100 mm/s (50–60 s), the cutting force also decreased [Fig. 10(c)], and the current decreased to 0.8 A [Fig. 10(d)].

Figures 11(a) and 11(b) present the force and current data obtained from EXP3, respectively. The results revealed that before cutting began (0–5 s), the spindle motor was idle, and its current was 1 A. After cutting began, the maximum cutting force and current reached 5 lbf and 1.18 A, respectively. Figures 12(a)–12(d) present the overall force, overall current, zoom-in force, and zoom-in current data obtained from EXP4, respectively. After the spindle motor was switched on, its rotation speed increased to 25000 RPM, and the current progressively increased to 1.25 A before decreasing and stabilizing at 0.9 A [Fig. 12(b)]. When the cutting force decreased [Fig. 12(c)], the motor current decreased to 0.89 A [Fig. 12(d)]. The slight difference observed between the cutting force and the current was attributed to the limitation of the sampling rate to 45 ms, which did not meet the required sampling rate for NI 9234. Consequently, the current data exhibited step-shaped patterns.

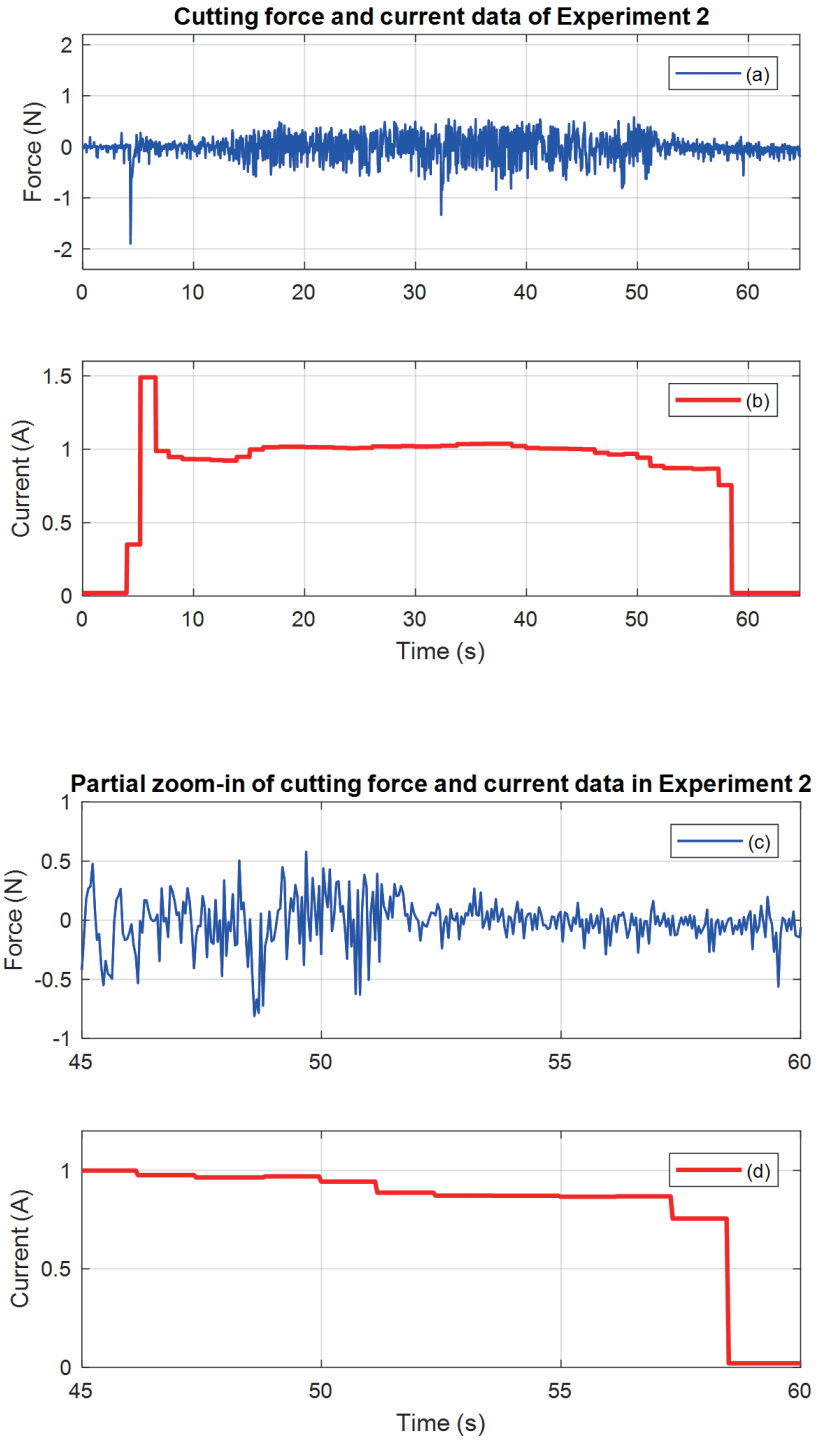

Fig. 10. (Color online) (a) Overall force, (b) overall current, (c) zoom-in force, and (d) zoom-in current data of EXP2.

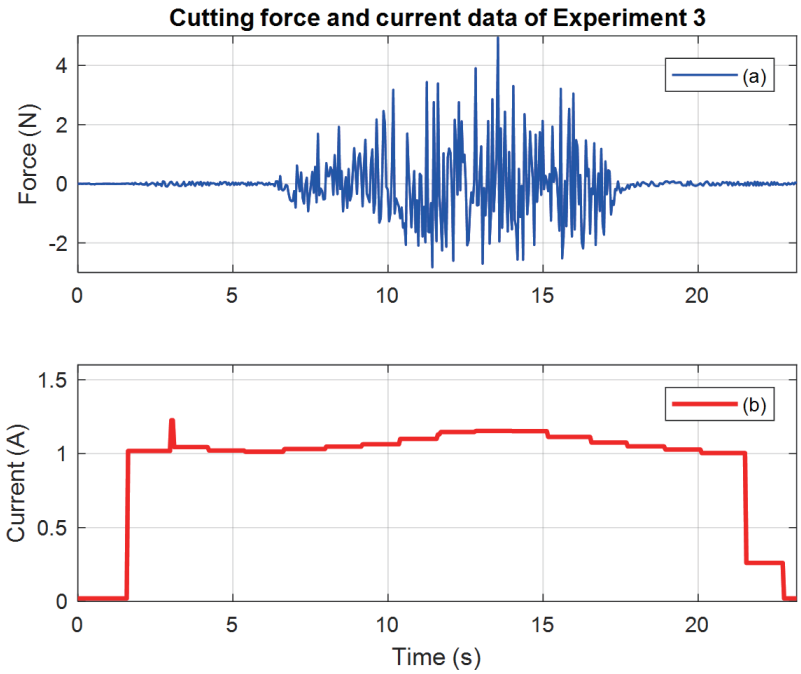

Fig. 11. (Color online) (a) Force and (b) current data of EXP3.

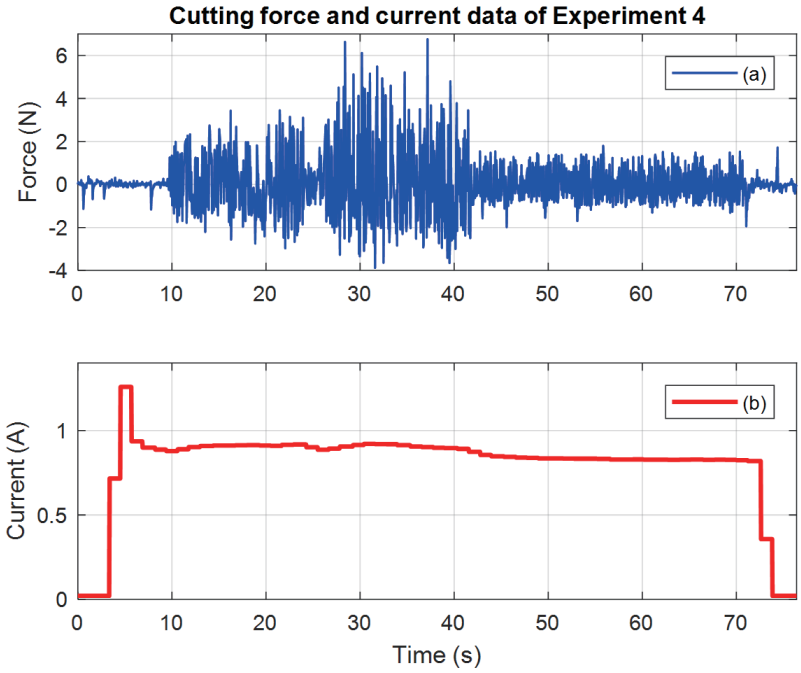

Fig. 12. (Color online) (a) Overall force, (b) overall current, (c) zoom-in force, and (d) zoom-in current data of EXP4.

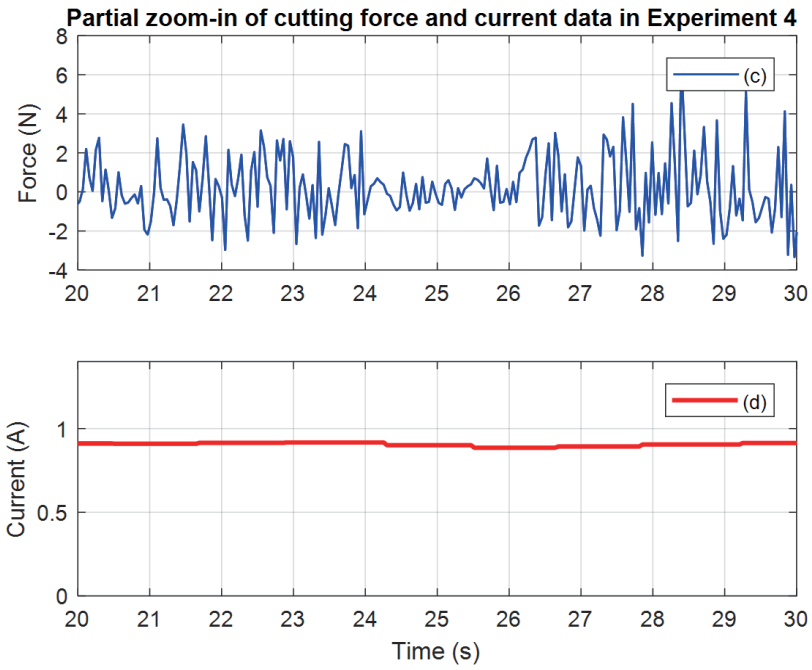

Fig. 12. (Color online) (Continued) (a) Overall force, (b) overall current, (c) zoom-in force, and (d) zoom-in current data of EXP4.

4. Experimental Results

Changes in spindle motor current were observed by using a robotic arm to cut propeller blades according to the framework presented in Fig. 5 and the flowchart presented in Fig. 6.

4.1. Software-based path planning

Before cutting was conducted, the cutting path was simulated by modeling the robotic arm, spindle motor, cutting tool length, cutting tool base, propeller, rotating platform, and end effector. RoboDK software was used to plan the cutting path, and the robotic arm underwent fine adjustment to ensure a smooth process. Figure 13 presents the path planned for cutting the propeller blades. Figure 14 depicts the safe height of the cutting tool and the various cutting points along the cutting path.

4.2. Actual cutting

A 3D-printed propeller made of polylactic acid was used as the machining workpiece. A coating of black plastic paint was applied to this workpiece to increase the visibility of the cutting path and the thickness of the propeller blades (Fig. 15). As shown in Fig. 16, the coating

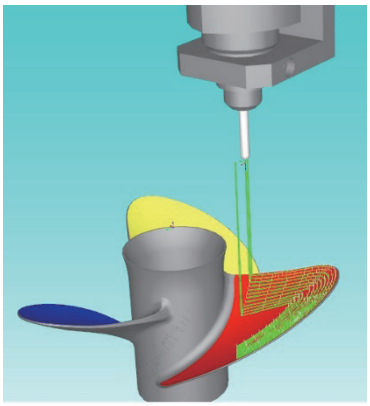

Fig. 13. (Color online) Planning of the cutting path.

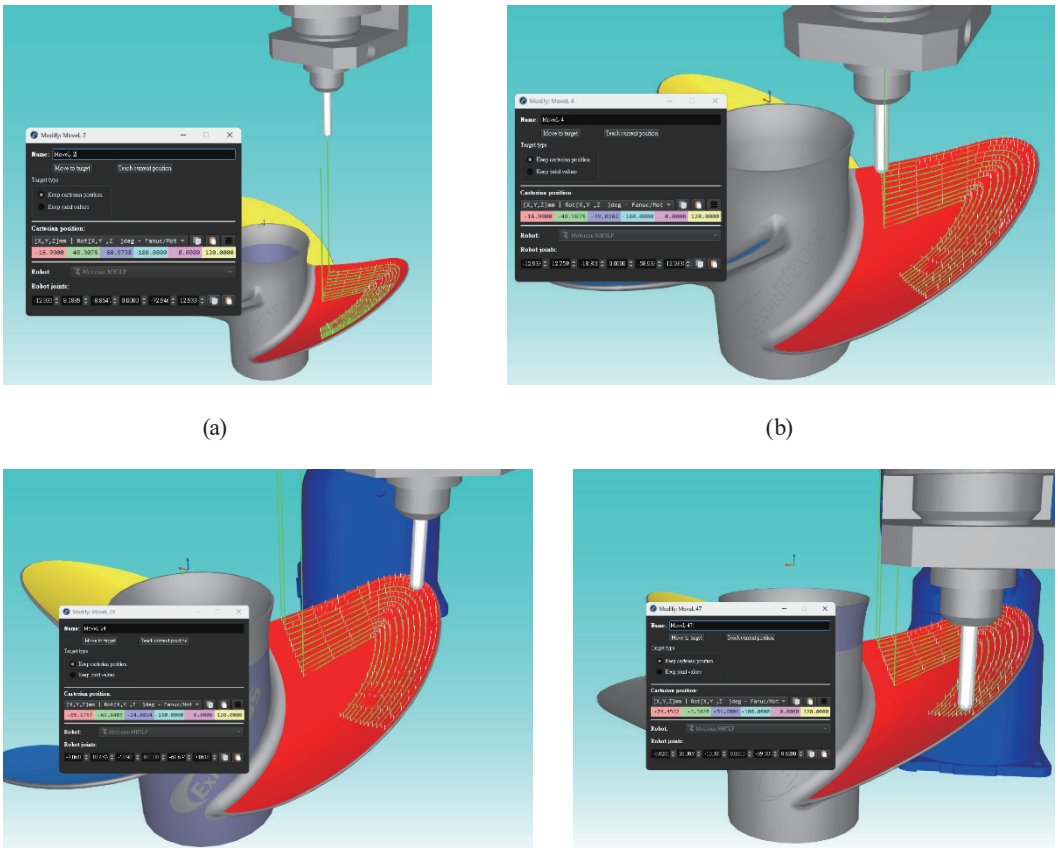

(a) (b)

(c) (d)

Fig. 14. (Color online) Illustration of the cutting path for creating the propeller blades. (a) Cutting tool safe height, (b) cutting point 1, (c) cutting point 2, and (d) cutting point 3.

Fig. 15. (Color online) Additional coating applied to the workpiece.

(a) (b) (c)

Fig. 16. (Color online) Actual cutting paths of propeller blades. (a) Path of Blade 1, (b) path of Blade 2, and (c) path of Blade 3

enhanced the visibility of the cutting tool mark on the workpiece. The cutting process was performed at a motor rotation speed of 25000 RPM, a feed rate of 50 mm/s, and a sampling rate of 45 ms. Table 3 lists the cutting depths of the three blades.

4.3. Discussion

When the cutting tool reached the first cutting point, Blade 1 was penetrated [Fig. 16(a)], and the motor current continued to increase (20–30 s), eventually reaching 1.28 A [Fig. 17(a)]. Accordingly, the process of cutting Blade 2 was adjusted by reducing the cutting depth by 1 mm. Therefore, Blade 2 was cut successfully [Fig. 16(b)], and the motor current continued to decrease throughout the cutting process [Fig. 17(b)] because when the cutting tool moved toward the propeller center, the contact surface between the tool and the workpiece decreased, reducing the cutting force and motor current. On the basis of this observation, the cutting depth of Blade 3

Table 3
Cutting depths of the propeller blades.

	Blade 1	Blade 2	Blade 3
Cutting depth	Aligned with the blade surface	Reduced depth by 1 mm in comparison with Blade 1	Reduced depth by 0.8 mm in comparison with Blade 1

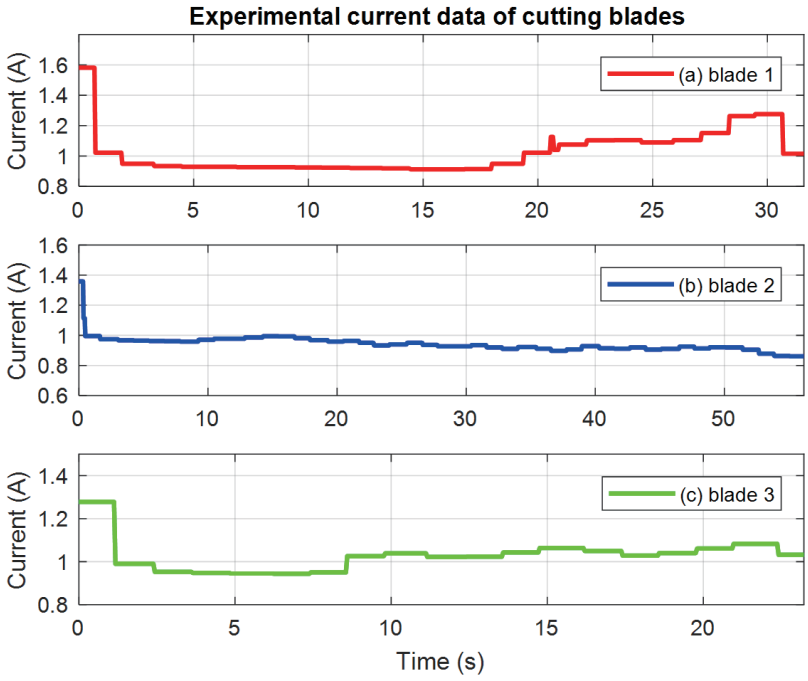

Fig. 17. (Color online) Experimental current data of cutting blades.

was reduced by only 0.8 mm. However, cracks appeared during cutting [Fig. 16(c)], and the motor current continued to increase [Fig. 17(c)], which was undesirable. This finding indicated that reducing the cutting depth by 0.8 mm still resulted in an excessively deep cut. In the experiment of cutting three blades, only the change in the current value of the motor spindle was measured. According to the data of EXP3 and EXP4 in Table 2, the cutting force should be between 2 and 3 N. By monitoring the changing trend of the current, the cutting force can be known, and the changes will provide important information to the processing manufacturer.

During machining, it is typically necessary to strike a balance between the feed rate and the cutting speed. Generally, increasing the feed rate and cutting speed can enhance machining efficiency, but considerations must also be given to factors such as tool life, surface finish quality, and machining stability. Therefore, in actual machining operations, it is important to select the appropriate feed rates and cutting speeds on the basis of specific machining requirements and conditions.

5. Conclusions

In this study, the simultaneous measurement of the cutting force and current was achieved using an inexpensive current sensor and a program developed using LabVIEW. Changes in spindle motor current with respect to cutting force were observed, and the proposed measurement scheme was applied in the physical production of a 3D-printed propeller.

Although the sampling rate of the inexpensive current sensor reached only 45 ms, which was considerably lower than the 10 ms sampling rate achieved through the integration of NI9234 and cDAQ-9171, changes in spindle motor current were still observed through the developed program, which was verified as a viable alternative to other measurement methods that require more costly force sensors. In summary, the proposed measurement scheme can achieve the real-time monitoring of cutting force through inexpensive equipment. In the future, the developed program will be combined with an embedded control system (NI compact RIO 9065) and artificial intelligence technology to further improve its capabilities to monitor the cutting force of a robotic arm in real time, to minimize the consumption of human resources, and to enhance machining quality.

Acknowledgments

The authors would like to thank the National Pingtung University for funding this study under Research Project Nos. 112T6201,112T0063, and 112T0065.

References

1 F. Nagata, K. Watanabe, and K. Izumi: IEEE Int. Conf. Robotics and Automation **1** (2001) 319. https://doi.org/10.1109/ROBOT.2001.1620978
2 Z. Dong, Y. Chao, S. Dezheng, L. Xiaodong, and W. Xiaozhi: IEEE Int. Conf. Mechanic Automation and Control Engineering (MACE). **26**–**28** (2010) 2470.
3 Y. Altintas: J. Eng. Ind. **114** (1992) 386. https://doi.org/10.1115/1.2900688.
4 D. Aslan and Y. Altintas: IEEE ASME Trans. Mechatron. **23** (2018) 833. https://doi.org/10.1109/TMECH.2018.2804859
5 Y.-H. Jeong and D.-W. Cho: Int. J. Mach. Tools Manuf. **42** (2002) 1559. https://doi.org/10.1016/S0890-6955(02)00082-2
6 H. Tanabi, N. Babaei, and A. Babaei: Adv. Mater. Res. **341**–**342** (2011) 307. https://doi.org/10.4028/www.scientific.net/amr.341-342.307
7 K. Miura, B. Döbbeler, and F. Klocke: Procedia CIRP **78** (2018) 323. https://doi.org/10.1016/j.procir.2018.09.068
8 X. Li, A. Djordjevich, and P. K. Venuvinod: IEEE Trans. Ind. Electron. **47** (2000) 697. https://doi.org/10.1109/41.847910
9 A. Matsubara and S. Ibaraki: Int. J. Automot. Technol. **3** (2009) 445. https://doi.org/10.20965/ijat.2009.p0445
10 Y.-M. Cheng: Materials **15** (2022) 2268. https://doi.org/10.3390/ma15062268
11 Y. M. Cheng, W. X. Peng, and A. C. Hsu: Int. J. Adv. Manuf. Technol. **76** (2015) 1253. https://doi.org/10.1007/s00170-014-6337-y